

# Chute flows of dry granular media: numerical simulations by a well-posed multilayer model and comparisons with experiments

Luca Sarno<sup>1,2\*</sup>, Yongqi Wang<sup>1</sup>, Yih-Chin Tai<sup>3</sup>, Maria Nicolina Papa<sup>2</sup>, and Paolo Villani<sup>2</sup>

<sup>1</sup>Chair of Fluid Dynamics, Dept. of Mechanical Engineering, Technical University of Darmstadt, 64287 Darmstadt, Germany

<sup>2</sup>Laboratory of Environmental and Maritime Hydraulics, Dept. of Civil Engineering, University of Salerno, 84084 Fisciano, Italy

<sup>3</sup>Dept. of Hydraulic and Ocean Engineering, National Cheng-Kung University, 70101 Tainan, Taiwan

**Abstract.** Debris flows and avalanches are dangerous natural phenomena, characterized by the gravity-driven motion of granular media immersed in a fluid. For an appropriate hazard assessment or disaster mitigation by scenario investigation, it is crucial to capture the underlying dynamics of the granular solid phase. For this purpose, a multilayer depth-averaged approach represents a promising and computationally efficient tool over fully three-dimensional models. Here we use a mathematically well-posed multilayer model, which implements the  $\mu(I)$ -rheology and a dilatancy law depending on the inertial number,  $I$ , and compare the numerical results of the model with laboratory experiments of steady uniform chute flows over an erodible bed. The well-posedness of the model for any value of  $I$ , which is essential to get convergent numerical solutions, is achieved by considering an approximation of the in-plane stress gradients, directly emerging from the  $\mu(I)$ -rheology. The predicted velocity profiles show a very good agreement with the experimental ones, measured by particle image velocimetry (PIV). The volume fraction profiles by the multilayer model are also in good qualitative agreement with those measured by using the stochastic-optical method (SOM), while they tend to overestimate the volume fraction measurements in the more dilute upper region, closer to the free surface.

## 1 Introduction

Debris flows and granular avalanches are dangerous phenomena for humans and infrastructures in mountainous regions. The physical understanding of the granular dynamics and the related mathematical modelling are essential for the risk assessment of such events. In the context of continuum mechanics, depth-averaged models, equipped with suitable constitutive laws, are widely employed for the description of granular flows, especially for large field-scale simulations (e.g., [1]), as they are computationally more efficient than three-dimensional (3D) models. Yet, depth-averaged models miss significant dynamical processes occurring along the transverse flow direction. While single-layer models are suitable for describing granular flows with a blunt velocity profile, they become insufficient if the velocity profiles are highly sheared and swiftly change in shape owing to a rheological stratification (e.g., [2]). The multilayer approach [3-5] represents a way to partially overcome the aforementioned limitations without renouncing the computational advantages of the depth-averaged models. In this work, we employ a mathematically well-posed multilayer model, introduced by [5], and compare the modelled velocity and volume fraction profiles with the experimental data of steady uniform chute granular flows over an erodible bed. The model uses the well established  $\mu(I)$ -rheology [6] and also incorporates a

dilatancy law, depending on the inertial number  $I$ , to take into account the effects of the variable volume fraction [7]. It is worth noting that the well-posedness of the model for any value of the inertial number,  $I$ , is also practically useful to obtain convergent numerical solutions [5]. For a suitable comparison with the experiments in a narrow chute, the multilayer model is here equipped with rate-independent Coulomb-friction terms accounting for the sidewall resistances (e.g., [8]). Fig. 1 shows a sketch of the multilayer approach, where the spatial domain of the granular avalanche is partitioned into a pre-set number,  $N$ , of layers that dynamically evolve according to the chosen rheology.

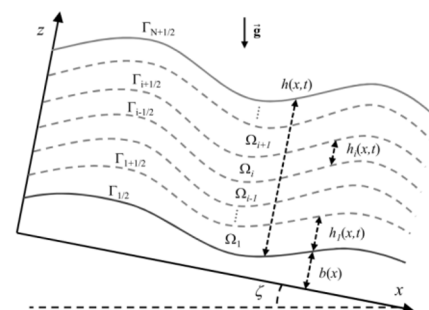


**Fig. 1.** Sketch of the multilayer approach [5], where the generic layer is represented by the symbol,  $\Omega_i$ , the layer thickness by  $h_i$ , and the layer interfaces by  $\Gamma_{i\pm 1/2}$ .

\*Corresponding author: [sarno@fdy.tu-darmstadt.de](mailto:sarno@fdy.tu-darmstadt.de)

## 2 Multilayer model equations and numerical integration

The model equations were obtained by depth-averaging the mass and momentum balances in each layer, followed by first-order asymptotic expansion for the parameter  $\varepsilon = H/L \ll 1$ , with  $H$  and  $L$ , respectively, being the typical depth and length scales of the avalanche. More details on the derivation of the model equations and its key mathematical properties can be found in [5]. A distinctive feature of the proposed multilayer model is that an approximation of the in-plane stress gradients, directly emerging from the  $\mu(I)$ -rheology, is considered in the layer-averaged momentum equations, to ensure the well-posedness for any  $I$ . It is worth noting that this additional term is smaller than the leading order approximation,  $O(\varepsilon)$ , and, thus, is usually neglected in the first-order depth-averaged models available in the literature [9]. With reference to the generic layer  $i$ , the model partial differential equations (PDE) are

$$\begin{aligned} \tau_{relax} \left( \partial_t \bar{v}_i + u_i^* \partial_x \bar{v}_i \right) &= \bar{v}_i - \overline{v_{i,EOS}}, \quad (1) \\ \partial_t \left( h_i \bar{v}_i \right) + \partial_x \left( h_i \bar{v}_i u_{x,i} \right) &= \frac{1}{\rho_g} \left( M_{x,i-1/2} - M_{x,i+1/2} \right), \quad (2) \\ \partial_t \left( h_i \bar{v}_i u_{x,i} \right) + \partial_x \left( \frac{\left( h_i \bar{v}_i u_{x,i} \right)^2}{h_i \bar{v}_i} \right) &+ \partial_x \left( \frac{g_x \left( h_i \bar{v}_i \right)^2}{2 \bar{v}_i} \right) \\ + g_z \left[ \frac{h_i \bar{v}_i}{\bar{v}_i} \partial_x \left( \sum_{j=i+1}^N \bar{v}_j h_j \right) + h_i \bar{v}_i \partial_x \left( \sum_{j=1}^{i-1} \frac{h_j \bar{v}_j}{\bar{v}_j} \right) \right] &= \\ g_x h_i \bar{v}_i - g_z h_i \bar{v}_i \partial_x b & \\ + \psi \partial_x \left( \bar{v}_i h_i \sqrt{\sum_{j=i+1}^N \bar{v}_j h_j + \frac{\bar{v}_i h_i}{2} \partial_x \left( \frac{h_i \bar{v}_i u_{x,i}}{h_i \bar{v}_i} \right)} \right) & \\ - \frac{1}{\rho_g} \left( \tilde{t}_{xz}^* \Big|_{i-1/2} - \tilde{t}_{xz}^* \Big|_{i+1/2} \right) & \\ + \frac{1}{\rho_g} \left( u_{i-1/2,downwind} M_{x,i-1/2} - u_{i+1/2,downwind} M_{x,i+1/2} \right) & \\ - 2 \frac{\mu_{side}}{W} g_z \left[ \sum_{j=i+1}^N \bar{v}_j h_j + \frac{\bar{v}_i h_i}{2} \right] \frac{h_i \bar{v}_i u_{x,i} / h_i \bar{v}_i}{\left[ h_i \bar{v}_i u_{x,i} / h_i \bar{v}_i \right]} & \end{aligned} \quad (3)$$

where  $g_x = g \sin \zeta$ ,  $g_z = g \cos \zeta$ ,  $\rho_g$  is the grain density,  $W$  is the channel width and  $\mu_{side}$  is a friction coefficient parameterizing the sidewall resistances. In (1)-(3) the unknowns are the layer-averaged volume fractions,  $\bar{v}_i$ , the layer masses,  $h_i \bar{v}_i$ , and the layer-averaged momenta,  $h_i \bar{v}_i u_{x,i}$ , with  $u_{x,i}$  denoting the  $x$ -component velocity in the layer  $i$ . Eq. (1) describes the transport of  $\bar{v}_i$  and its concurrent relaxation toward the equilibrium value,  $\overline{v_{i,EOS}}$ , according to a relaxation time,  $\tau_{relax}$  [5]. The dilatancy law, here used for defining  $\overline{v_{i,EOS}}$ , represents a slight modification of the formula proposed by [7] for dense granular flows,

$$v(I) = v_{min} + \frac{v_{max} - v_{min}}{1 + a' I}. \quad (4)$$

In (4)  $a'$  is an empirical parameter,  $v_{min}$  and  $v_{max}$  are, respectively, the lower and upper bounds for  $v$  [5]. Eq. (2) is the mass balance of the generic layer  $i$ , where  $M_{x,i\pm 1/2}$  are the mass fluxes per unit length of interface projected along  $x$ , which can be set equal to zero for the case of immiscible layers or calculated by suitable closures. Finally, Eq. (3) is the momentum balance equation of the layer  $i$ . In (3),  $\psi = d_g (\mu_s + \mu_2) \sqrt{g_z} / I_0 v_0$ , with  $d_g$  being the grain diameter, is a diffusion-like coefficient accounting for the effects of the in-plane stress gradients, and ensures the well-posedness of the model for all  $I$  [5]. The shear stresses,  $\tilde{t}_{xz}^* \Big|_{i\pm 1/2}$ , in (3) are calculated by suitable discretizations of the  $\mu(I)$ -rheology [5],

$$\mathbf{T}^* = \frac{\sqrt{2} \left( \mu_s + \frac{\mu_2 - \mu_s}{I_0 / I + 1} \right) p}{\|\mathbf{D}\|} \mathbf{D}. \quad (5)$$

In (5)  $\mathbf{T}^*$  is the shear-stress tensor,  $\mathbf{D}$  is the strain-rate tensor,  $\|\cdot\|$  is the Frobenius norm,  $p$  is the pressure,  $\mu_s$  is the static friction coefficient,  $\mu_2$  is an upper bound for  $\mu$ , and  $I_0$  is a constant [6].

The PDE system, (1)-(3), is numerically integrated by means of an operator splitting scheme, where its advection part is advanced by a finite volume scheme, employing a lateralized Harten–Lax–van Leer (LHLL) approximate Riemann solver [10]. High resolution in space is achieved thanks to a MUSCL predictor-corrector treatment. More details on the numerical scheme can be found in [5].

## 3 Comparisons with experimental data and discussion

The predictions by the multilayer model are compared with the steady uniform velocity and volume fraction profiles of chute flow experiments over an erodible bed, carried out at the University of Salerno (Italy).

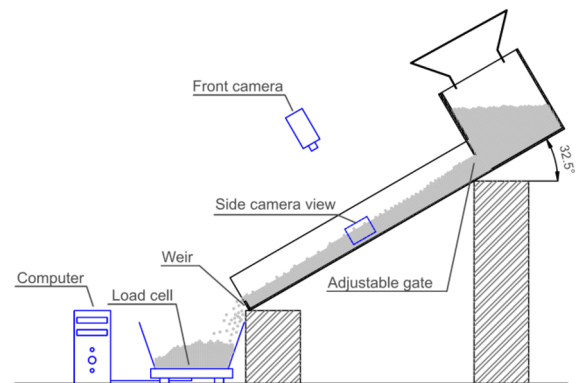


**Fig. 2.** The experimental set up.

The laboratory setup, similar to that used in [11], is composed of a 2-m-long Plexiglas chute with a width,

$W = 80\text{mm}$ , and an inclination of  $32.5^\circ$  (Fig. 2). A 6-cm-high weir was placed at the chute outlet to enforce the formation of a static wedge of granular material below the active surface flow. The granular material, composed of polyoxymethylene (POM) spheroidal beads with diameter,  $d_g = 3.3\text{mm}$ , was initially stored in the upper part of the chute and then flowed down through an adjustable gate. Different flow rates and flow regimes were investigated by adjusting the gate opening between 6 cm and 14 cm. Despite the fact that the flume inclination was fixed ( $32.5^\circ$ ), the inclination of the free surface of the granular flow, as well as the one of the erodible bed, was found to self-adjust depending on the mass flow rate. For each experiment, a transient of a few seconds was followed by a steady state regime, in which the fully developed surface flow was superimposed on a static granular wedge. In an intermediate region of the flume far enough from the inlet and the outlet, almost uniform flow conditions were observed. The measurements were taken at a cross section, 1 m downstream from the gate, by means of two high-speed cameras (AOS Technologies Corp.) capable of recording 1000 frames per second. The sidewall velocity profiles were obtained using the particle image velocimetry (PIV) open-source package PIVlab [12], and a 4-pass PIV analysis was carried out [13]. The velocity field at the free surface, captured by the front camera, allowed the estimation of a homogenization coefficient,  $\alpha$ , accounting for the deviations from a purely 2D flow (e.g., [11, 14]), and, consequently, permitted the estimation of the width-averaged velocity profiles, which are directly compared with the computed profiles by the model.

The volume fraction profiles near the sidewall were measured using the stochastic-optical method (SOM) [15]. This method, based on a binarization of the photographs taken by the side camera, uses a stochastic transfer function, previously obtained by Monte Carlo simulations, and requires controlled illumination conditions. In this application, a no-flicker LED lamp (PhotoSonics MultiLED-LT) was placed at a distance of 32cm and with an incidence angle of  $25^\circ$  with respect to the normal to the sidewall. To ensure the reliability of measurements, the velocity and volume fraction profiles were estimated by time-averaging the measurements over a time interval of 5 seconds, and also by averaging over 4 repetitions of the same experiment.

The simulations by the multilayer model were conducted on a time interval of 25s, such that fully developed flows occurred for all runs. The simulations started from an initially static deposit with an arbitrary thickness,  $h$ , which was made to flow on a bed inclination,  $\zeta$ , equal to the inclination of the erodible bed in the experiment to be described. Namely, the initial conditions are

$$\begin{aligned} h &= \sum_{i=1}^N h_i(x, 0) = 0.099\text{m}, \\ \bar{u}_i(x, 0) &= 0, \quad \bar{v}_i(x, 0) = 0.6. \end{aligned} \quad (6)$$

A spatial domain,  $x \in [-0.5, 0.5]\text{m}$ , is considered with a no-slip bed kinematic condition and non-reflecting boundaries at  $x = -0.5\text{m}$  and  $x = 0.5\text{m}$ . All the

simulations were performed with a number of layers,  $N = 60$ , and a spatial discretization,  $\Delta x = 0.1\text{m}$ . The time step was chosen equal to  $\Delta t = 0.002\text{s}$ , fulfilling the Courant-Friedrichs-Lewy (CFL) condition for all the investigated flows. The following rheological parameters were employed:  $\mu_s = \tan(27.0^\circ)$ ,  $\mu_2 = \tan(32.8^\circ)$ ,  $I_0 = 0.55$ ,  $\mu_{side} = \tan(10.4^\circ)$ , while the dilatancy law, (4), was used with the following parameters:  $\nu_{min} = 0.2$ ,  $\nu_{max} = 0.6$  and  $a' = 0.5$ .

With reference to the intermediate run, characterized by an inflow gate opening of 8cm and representative of the entire data set, Fig. 3 illustrates the velocity and volume fraction profiles computed by the model and the experimental ones. As it is clear from Fig. 3(a), the agreement between the numerical and experimental velocity profiles is excellent. Minor discrepancies are observed in the lower creep region ( $h - z \leq -0.03\text{m}$ ), where the model slightly underestimate the experimental velocities.

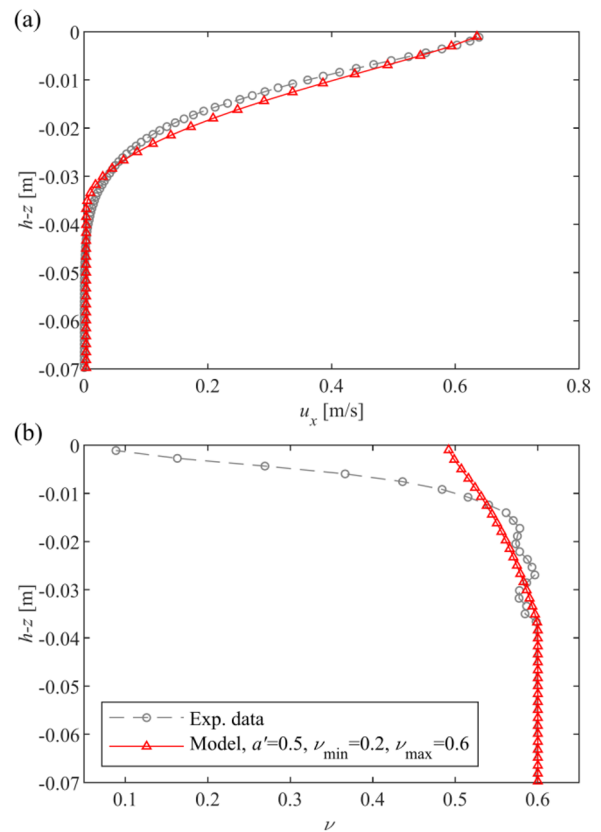


**Fig. 3.** Comparisons between the steady uniform profiles predicted by the multilayer model (at  $t=25\text{s}$ ) and the experimental ones (experiment with inflow gate opening 8cm): (a)  $x$ -component velocity,  $u_x$  (b) volume fraction,  $\nu$ .

This is probably due to the chosen rheological assumptions ( $\mu(I)$ -rheology and Coulomb-friction for the sidewall resistances), which predict zero velocity from a fixed depth, while the actual behaviour of the lower creep flow consists of an exponential tail [16]. Focusing on the volume fraction profiles (Fig. 3(b)), it can be noted that the model with the dilatancy law, (4), qualitatively reproduces the general trend of the experimental  $\nu$  profile. Yet, it is unable to correctly

describe the upper, more dilute flow region, corresponding to a thickness of a few grain diameters ( $\approx 0.01\text{m}$ ). This disagreement suggests that the chosen dilatancy law, (4), is probably no longer valid in the dilute regime.

The reported study on chute flows over an erodible bed confirms the good capabilities of the multilayer approach to reproduce the velocity and volume fraction fields of dry granular avalanches. Especially considering its relatively low computational costs [5], the multilayer approach represents a valuable tool to regularize and approximate more computationally expensive 3D models based on similar rheological assumptions. Moreover, the versatility of the multilayer framework would allow the future implementation of more sophisticated dilatancy laws without much effort.

This work is part of the project, "StratifiedGRANULAR", which received funding from the European Union's Horizon 2020 research and innovation programme under the Marie Skłodowska-Curie grant agreement No. 797890.

## References

1. R. M. Iverson, *Rev. Geophys.*, **35**(3), 245-296 (1997)
2. A. Armanini, H. Capart, L. Fraccarollo, M. Larcher, *J. Fluid. Mech.*, **532**, 269–319 (2005)
3. E. Audusse, *Discrete Cont. Dyn. B*, **5**(2), 189-214 (2005)
4. E. D. Fernández-Nieto, J. Garres-Díaz, A. Mangeney, G. Narbona-Reina, *J. Fluid Mech.*, **798**, 643-681 (2016)
5. L. Sarno, Y. C. Tai, Y. Wang, M. Oberlack, *Phys. Fluids*, **33**(10), 103319 (2021)
6. P. Jop, Y. Forterre, O. Pouliquen, *Nature*, **441**(7094), 727-730 (2006)
7. F. da Cruz, S. Emam, M. Prochnow, J. N. Roux, F. Chevoir, *Phys. Rev. E*, **72**(2), 021309 (2005)
8. A. W. Roberts, *ASME Trans. J. Eng. Ind.*, **91**, 373-381 (1969)
9. J. M. N. T. Gray, A. N. Edwards, *J. Fluid Mech.*, **755**, 503 (2014)
10. L. Fraccarollo, H. Capart, Y. Zech, *Int. J. Numer. Meth. Fl.*, **41**(9), 951-976 (2003)
11. L. Sarno, L. Carleo, M. N. Papa, P. Villani, *Rock Mech. Rock Eng.*, **51**(1), 203-225 (2018)
12. W. Thielicke, E. J. Stamhuis, *J. Open Res Soft.*, **2**(1), e30 (2014)
13. L. Sarno, A. Carravetta, Y. C. Tai, R. Martino, M. N. Papa, C. Y. Kuo, *Adv. Powder Technol.*, **29**(12), 3107-3123 (2018)
14. L. T. Sheng, C. Y. Kuo, Y. C. Tai, S. S. Hsiau, *Exp. Fluids*, **51**(5), 1329-1342 (2011)
15. L. Sarno, M. N. Papa, P. Villani, Y. C. Tai, *Granul. Matter*, **18**(4), 1-12 (2016)
16. T. S. Komatsu, S. Inagaki, N. Nakagawa, S. Nasuno, *Phys. Rev. Lett.*, **86**(9), 1757 (2001)